



STRUCTURAL SCIENCE
CRYSTAL ENGINEERING
MATERIALS

ISSN 2052-5206

A new olanzapine cocrystal obtained from volatile deep eutectic solvents and determined by 3D electron diffraction

Iryna Andrusenko,^a Jason Potticary,^b Simon R. Hall^{b*} and Mauro Gemmi^{a*}

Received 15 July 2020

Accepted 20 September 2020

Edited by J. Hadermann, University of Antwerp, Belgium

Keywords: olanzapine; eutectic solvent; electron diffraction; crystal structure; centrosymmetric dimer; VODES.

CCDC references: 2027602; 2030951

Supporting information: this article has supporting information at journals.iucr.org/b

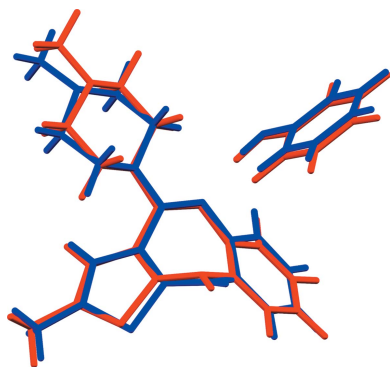
^aCenter for Nanotechnology Innovation@NEST, Istituto Italiano di Tecnologia, Piazza San Silvestro 12, Pisa, Italy, and ^bSchool of Chemistry, University of Bristol, Cantock's Close, Bristol, BS8 1TS, United Kingdom. *Correspondence e-mail: simon.hall@bristol.ac.uk, mauro.gemmi@iit.it

A previously unknown cocrystal of olanzapine and phenol was identified from a volatile deep eutectic solvent as the intermediate species in the crystallization of olanzapine. This new nanocrystalline phase was investigated by electron diffraction, powder X-ray diffraction and differential scanning calorimetry. The structure was determined by simulated annealing using 3D electron diffraction data and confirmed using DFT-D optimizations. Olanzapine and phenol cocrystallize in the triclinic space group $P\bar{1}$, supporting the hypothesis of a dimeric growth unit, where a centrosymmetric dimer is stabilized by multiple weak C—H $\cdots\pi$ interactions and forms double N—H \cdots N hydrogen bonding with adjacent dimers.

1. Introduction

Olanzapine [2-methyl-4-(4-methylpiperazin-1-yl)-10*H*-thieno[2,3-*b*][1,5]benzodiazepine] is an atypical antipsychotic drug that has proven efficacy against the positive and negative symptoms of schizophrenia, bipolar disorder and related psychoses (Fulton & Goa, 1997; Bhana *et al.*, 2001). Olanzapine was first discovered while searching for a chemical analogue of clozapine that would not require haematological monitoring (Bitter *et al.*, 2004). However, increasing experience with atypical antipsychotics in real-world clinical environments has demonstrated that these drugs have a strong correlation with certain metabolic side effects, including weight gain, diabetes and dyslipidaemia (Rojo *et al.*, 2015). Switching or combining different agents may be sufficient in some cases for reducing these undesired side effects, but in most instances, additional drug treatments are required. Therefore, the development of antipsychotic medications that offer the efficacy of olanzapine but reduce the associated risks could address a major unmet need in the treatment of different schizophreniform disorders (Citrome *et al.*, 2019). Olanzapine–phenol cocrystal (Fig. 1) represents a typical case of an intermediate product obtained during drug manufacture. The detailed investigation of intermediate phases allows for a better understanding of crystallization pathways and may play a prominent role in the future development of organic and inorganic chemistry (Andrusenko *et al.*, 2011).

Olanzapine is a molecule that crystallizes with rich structural variety, having over 60 related structures reported in the Cambridge Structural Database (Groom *et al.*, 2016). There are several olanzapine anhydrous polymorphic forms (Wawrzycka-Gorczyca *et al.*, 2004; Thakuria & Nangia, 2011; Askin *et*



© 2020 International Union of Crystallography

al., 2019), as well as many hydrates (Capuano *et al.*, 2003; Reutzel-Edens *et al.*, 2003), solvates (Bojarska *et al.*, 2013), cocrystals (Nanubolu & Ravikumar, 2017) and salts (Sarmah *et al.*, 2016), obtained by diverse manufacturing processes. Additionally, computed crystal energy landscape screenings have shown that other forms of olanzapine are possible (Bhardwaj *et al.*, 2013).

Volatile deep eutectic solvents (VODES) have recently demonstrated their potential in reaching hard-to-access crystal polymorphs in other pharmaceutical systems (Andrusenko *et al.*, 2019; Potticary *et al.*, 2020), often under ambient conditions. In accordance with typical eutectic solvents, VODES are a mixture of a hydrogen-bond donor and acceptor. However, unlike typical eutectic solvents, one of these coformers is volatile and easily escapes the system, while the remaining stable component forms a crystalline product. When a new polymorph is formed *via* VODES it is common for the crystal size to be in the micro- and nanometre range, making standard crystallographic investigations for structure solution a challenge.

The most efficient method for recognizing and understanding the intermolecular interactions that produce a given polymorph is in the determination of its three-dimensional (3D) atomic structure. For crystals of size 0.1 mm or larger, single-crystal X-ray diffraction (XRD) is the method of choice, while for smaller crystals, powder XRD is often the only feasible option. However, powder XRD may fail due to accidental and systematic overlap of independent reflections even at medium resolution, which is emphasized if coherent crystalline areas are small or if the sample contains multiple phases. For poorly crystalline organic compounds, powder diffraction patterns often show only a few intense peaks at low angles, while the diffraction intensity decays quickly, even at medium resolution, eventually becoming part of the noise. Consequently, polymorphic modifications associated with nanocrystals are hard to identify. In these cases, 3D electron diffraction (3D ED) has proved to be a reliable method for structure determination, even when only micrometre- or submicrometre-sized single crystals are available (Gemmi *et al.*, 2019).

To fully exploit the potentialities of both powder XRD and 3D ED, we have adopted the following protocol: (i) any new synthesis is first characterized by powder XRD; (ii) if the pattern cannot be fully indexed with known structures, 3D ED

data are collected from several crystals to identify the phase (or phases) present in the sample and to measure the related unit cell(s); (iii) if unknown phases are detected, their crystal structures are determined by 3D ED and refined by Rietveld refinement against powder XRD. This method was also used in the case of olanzapine–phenol cocrystal.

The olanzapine molecule consists of three fused rings (benzene, diazepine and thiophene) and one additional satellite ring (piperazine) (Fig. 1*a*). The boat conformation of the central seven-membered diazepine ring defines the overall shape of the molecule. The disparity between the number of hydrogen-bond donors to acceptors makes olanzapine highly amenable to the inclusion of solvents in order to balance the hydrogen bonds (Infantes *et al.*, 2007). Phenol (Fig. 1*b*) is a simple molecule that has been widely explored and is often used in eutectic systems for pharmaceutical applications. It can act as both a hydrogen-bond donor and acceptor (Duarte *et al.*, 2017).

In the search for new olanzapine polymorphs by crystallization from VODES, we obtained a new intermediate crystalline complex of olanzapine and phenol. This phase appeared as submicrometre-sized grains and was therefore structurally characterized by 3D ED.

2. Experimental

2.1. Crystallization

Olanzapine–phenol cocrystals were grown using the VODES method (Potticary *et al.*, 2020). Solid olanzapine and phenol were mixed at a 1:8 ratio and left to spontaneously form a liquid at room temperature. This liquid was then dropped onto a glass surface and left to crystallize over a period of 24 h in a well-ventilated area, resulting in a white crystalline powder. Initially, the crystallinity of the sample was ascertained using an optical microscope with cross-polarized filters.

2.2. Proton NMR

¹H NMR spectroscopic analysis was conducted using a Jeol ECS 400 NMR spectrometer. Spectra were obtained from about 10 mg of sample dissolved in 1 ml of dimethyl sulfoxide-*d*₆ (Sigma–Aldrich, 99.5%). All spectra were analysed using *Mnova* software (Version 14.0.1-23559; Mestrelab Research).

2.3. Thermal investigation

Melting points were recorded using differential scanning calorimetry (DSC) and the investigation was carried out using a TA Instruments Discovery DSC25 instrument. The cell was purged with N₂ gas at a rate of 50 ml min^{−1}. Samples weighing 2–10 mg were sealed in hermetically sealed T_{zero} aluminium pans. Starting at 30°C, samples were heated to temperatures at least 10°C above the observed endotherms. *TRIOS* software (Version 4.5.0.42498) was used for the analysis of the thermograms. Temperature and cell-constant calibrations were carried out using a certified indium standard (verification: $T = 156.6 \pm 0.5^\circ\text{C}$, enthalpy = $28.72 \text{ J g}^{-1} \pm 4\%$).

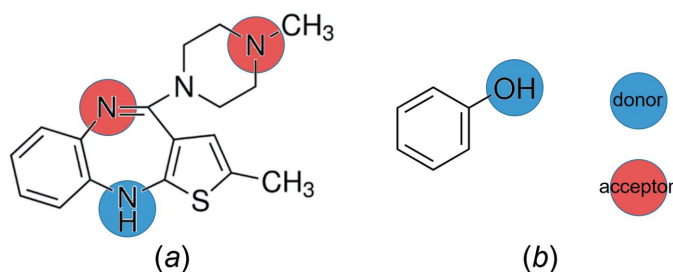


Figure 1
Molecular diagrams of (a) olanzapine and (b) phenol. Donor and acceptor groups are highlighted.

2.4. Electron microscopy and 3D electron diffraction

Scanning electron microscopy (SEM) micrographs were taken on a Jeol IT300 instrument using an accelerating voltage of 30 kV and samples were sputter coated with 15 nm of silver. High-angle annular dark-field scanning transmission electron microscopy (HAADF-STEM) imaging and electron diffraction (ED) data were recorded with a Zeiss Libra TEM operating at 120 kV and equipped with an LaB₆ source.

3D ED was performed in the same microscope in STEM mode after defocusing the beam in order to have a pseudo-parallel illumination on the sample, as described in Lanza *et al.* (2019). ED patterns were collected in Köhler parallel illumination with a beam size of about 150–200 nm in diameter, obtained using a 5 µm C2 condenser aperture. Data were recorded with a single-electron ASI MEDIPIX detector (Georgieva *et al.*, 2011). An extremely low dose illumination, corresponding to $0.01 \text{ e}^- \text{ Å}^{-2} \text{ s}^{-1}$, was adopted in order to avoid beam damage. The total dose during data collection depends on many experimental parameters, such as the number of frames, the exposure time and the image tracking mode, and is therefore different for each data collection. A rough estimation of the total dose during a stepwise data collection is in the $1\text{--}5 \text{ e}^- \text{ Å}^{-2}$ range, provided that the data are recorded with a single-electron detector. With a standard CCD, like our TRS $2k \times 2k$ model, the dose should be at least one order of magnitude higher.

The sample was crushed gently and loaded directly on a carbon-coated Cu TEM grid without any solvent or sonication. 3D ED acquisitions were performed when rotating the

sample around the TEM goniometer axis in steps of 1° , with a total tilt range from 65° to 100° . The exposure time per frame was 1 s. The camera length was 180 mm, allowing resolution in real space up to 0.7 Å . After each tilt, a diffraction pattern was acquired and the crystal position was tracked by STEM imaging (Gemmi & Lanza, 2019). During the experiment, the beam was precessed around the optical axis by an angle of 1° . Precession was obtained using a Nanomegas Digistar P1000 device. All data acquisitions were performed at room temperature.

3D ED data were analysed using the *PETS* software (Palatinus *et al.*, 2019). Structure determination was achieved by simulated annealing (SA), as implemented in the *SIR2014* software (Burla *et al.*, 2015). The resolution limit was set at 1.0 Å . SA is a stochastic algorithm that searches for the minimum of the cost function, gradually reducing the degrees of freedom (Kirkpatrick *et al.*, 1983). This global optimization method works especially well for organic compounds, where the symmetry is generally low, no atoms are in special positions and there are strict geometrical constraints imposed by intramolecular chemical bonding. For SA structure determination, the molecular model can be built considering the known chemical fragments or deduced from known polymorphic forms already reported in crystal structure databases. Each molecule can be modelled as a unique fragment, where the atomic distances and coordination are known. This method was applied successfully to 3D ED data for the determination of a covalent organic framework (Zhang *et al.*, 2013) and important pharmaceuticals (Das *et al.*, 2018). Olanzapine–phenol cocrystal appears as an ideal case for SA because the olanzapine molecule has only one free torsion angle, while the phenol molecule is entirely rigid.

Data were treated with a fully kinematical approximation, assuming that I_{hkl} was proportional to $|F_{hkl}|^2$. The model determined by SA was refined with the least-squares procedures embedded in the *SHELXL* software (Sheldrick, 2015). Geometrical restraints and constraints were added stepwise to check the consistency of the model. All H atoms were generated in geometrically idealized positions.

2.5. Powder X-ray diffraction

Powder XRD data were acquired in Debye–Scherrer geometry using a Stoe Stadi P diffractometer equipped with $\text{Cu K}\alpha_1$ radiation ($\lambda = 1.5406 \text{ Å}$), a Ge(111) Johansson monochromator from Stoe & Cie and a MYTHEN2 1 K detector from Dectris. The sample was loaded in a borosilicate glass capillary (0.5 mm external diameter) and data were acquired in the 2θ range $5\text{--}50^\circ$ with an interval of 0.003° between consecutive points. Data were processed with *GSAS-II* (Toby & Von Dreele, 2013).

2.6. Density functional theory (DFT) optimization

DFT calculations were performed with *CRYSTAL17* (Dovesi *et al.*, 2018) at the 6-31G level, using a Perdew–Burke–Erzerhof (PBE0-d3) exchange correlation functional with semi-empirical dispersion corrections (DFT-D) to

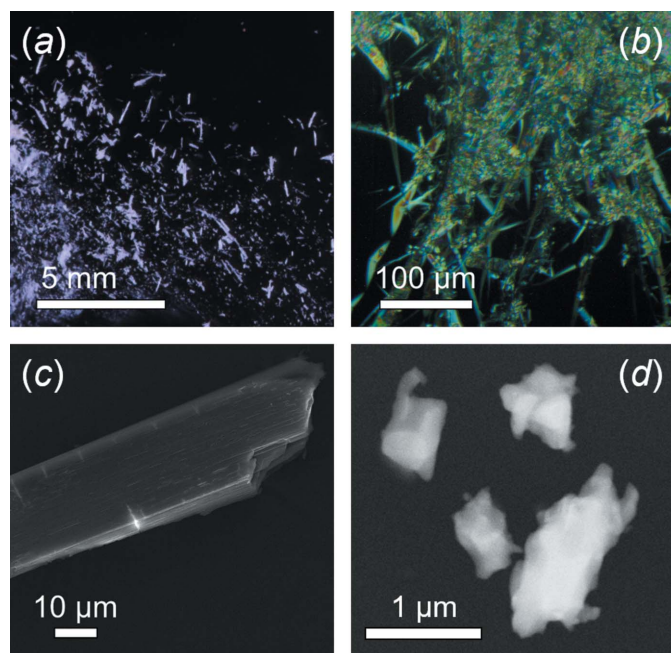


Figure 2

(a) Optical image of the white polycrystalline sample, (b) the same sample viewed through an optical microscope with cross-polarized filters, (c) SEM micrograph of a typical crystal showing the layered structure and (d) a HAADF-STEM image of typical olanzapine–phenol cocrystals used for 3D ED data collection.

account for van der Waals interactions; van der Waals radii were used as suggested by Grimme (2006) and Federov *et al.* (2012). Both the space group and the atomic coordinates obtained from 3D ED were used as the input geometry.

3. Results and discussion

3.1. Crystallization of a new cocrystal

The growth of olanzapine–phenol cocrystal from a VODES resulted in a white powder with a needle diameter size in the range 5–30 μm (Fig. 2*a*). The powder is visible under cross-polarized light and undergoes extinction at 90° intervals, revealing an anisotropic crystalline nature (Fig. 2*b*). SEM analysis shows that the needles are themselves layered (Fig. 2*c*), implying that an individual needle, if correctly isolated, would still be unsuitable for single-crystal structure solution.

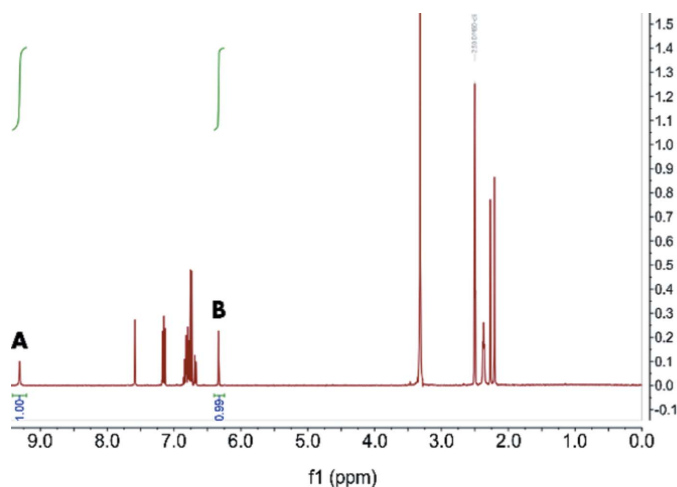


Figure 3
 ^1H NMR spectra in $\text{DMSO}-d_6$, showing the 1:1 ratio of the phenol hydroxy (A) and the olanzapine (B) single sp^2 -bound thiophene proton.

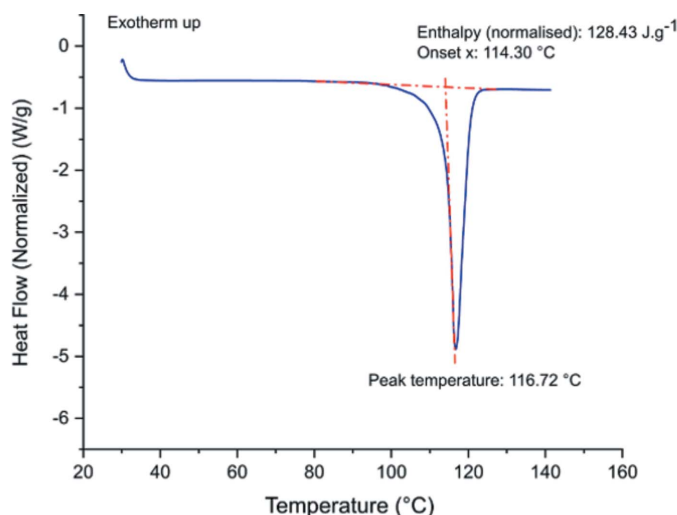


Figure 4
DSC thermogram of olanzapine–phenol cocrystal.

Analysis using ^1H NMR spectroscopy shows a molar ratio of olanzapine-to-phenol of 1:1 phenol hydroxy and thiophene protons integrating to 1.00 and 0.99, respectively (Fig. 3).

Thermal analysis of the cocrystal (Fig. 4) shows a single melting point of 114.3°C, with no evidence of a phenol melt at the expected temperature of 40.5°C. Unfortunately, due to the boiling point of phenol being 180.7°C, the temperature at which olanzapine is expected to melt (195°C) was not reached. This melt sits almost exactly between the melting points of the components (phenol and olanzapine melt at 40.5 and 195°C, respectively). This linear trend in physical properties is not unexpected in a 1:1 cocrystal, which distinguishes the structure from other disordered multicomponent solids like typical solvates or clathrates.

3.2. 3D ED structure analysis

3D ED data were recorded from three crystal fragments with sizes less than 1 μm (Fig. 2*d*). Unfortunately, we cannot provide an accurate estimation of the crystal thickness. Taking into consideration that all the observed crystals were not truly flat; their thicknesses were roughly estimated at about 50 nm. All 3D ED data sets were consistent with a triclinic cell, with approximate parameters $a = 9.0$, $b = 10.5$, $c = 12.0$ Å, $\alpha = 95^\circ$, $\beta = 95^\circ$ and $\gamma = 103^\circ$ (Fig. 5). Unit-cell parameters were refined and validated with a Pawley fitting against powder XRD data from which we obtained the refined lattice parameters $a = 9.4051$ (9), $b = 10.4236$ (11), $c = 11.999619$ (8) Å, $\alpha = 96.686$ (4), $\beta = 95.288$ (3) and $\gamma = 104.474$ (3)°. Taking into consideration the 1:1 ratio of olanzapine and phenol, such a cell would conveniently host two pairs of molecules ($Z = 2$). A close look at 3D ED reconstructions revealed no extinction features, pointing convincingly to a triclinic space group, *i.e.* $P1$ (No. 1) or $P\bar{1}$ (No. 2).

Structure solution was performed by SA using the highest quality (the most complete with the highest angular range and greatest resolution) 3D ED data set as an input. This global optimization method is the most frequently used and the only one so far to be applied to tomographic ED data (Zhang *et al.*, 2013; Das *et al.*, 2018). The two other data sets were of lower quality; therefore, the merging of data was not applied so as not to reduce the quality of the merged intensities. The merging of initially relatively poor 3D ED data only makes sense when, taken alone, each 3D ED data set lacks sufficient completeness for structure determination. A data completeness of 55% was enough to obtain a stable SA solution in a resolution range from 1.0 to 2.0 Å. This is also consistent with the results reported by Das *et al.* (2018) for other organic structures. Therefore, we avoided the merging of our three individual data sets into a unique data set, which would anyway be affected by random noise introduced by the different contributions of dynamical effects related to the different dimensions and shapes of the crystals. After the SA runs, the best crystallochemical model in the space group $P\bar{1}$ (No. 2) was taken as the initial model for further refinements.

The structure of olanzapine–phenol cocrystal was eventually refined *via* least squares against the 3D ED data,

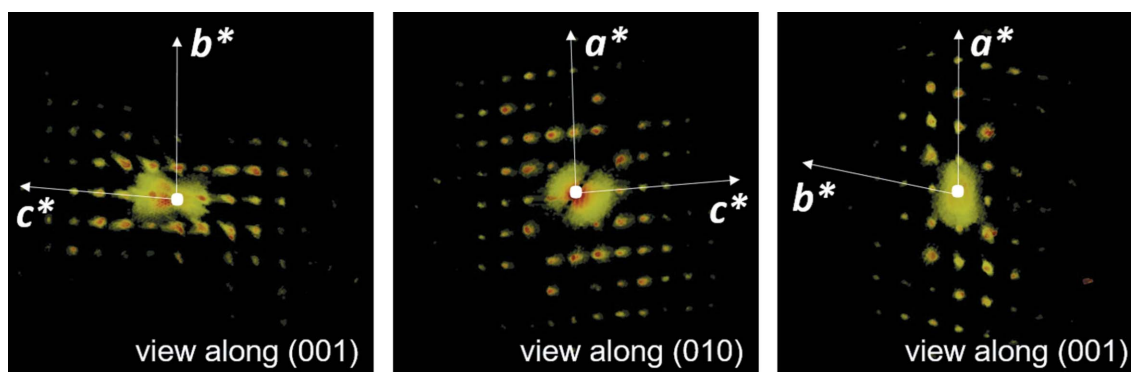


Figure 5
Reconstructions of the 3D ED volume viewed along the main crystallographic directions.

Table 1

Selected parameters from structure solution (*SIR2014*; Burla *et al.*, 2015) and refinement (*SHELXL*; Sheldrick, 2015) based on the 3D ED data.

Crystallographic information	
Asymmetric unit content	$C_{17}H_{20}N_4S \cdot C_6H_6O$
<i>Z</i>	2
Space group	$P\bar{1}$
<i>a</i> (Å)	9.4051 (9)
<i>b</i> (Å)	10.4236 (11)
<i>c</i> (Å)	11.9619 (8)
α (°)	96.686 (4)
β (°)	95.2878 (27)
γ (°)	104.474 (3)
Volume (Å ³)	1118.75 (5)
Structure solution parameters (<i>SIR2014</i>)	
Data resolution (Å)	1.0
No. of sampled reflections	2489
No. of independent reflections	1271
Independent reflections coverage (%)	55
Global thermal factor U_{iso} (Å ²)	0.04053
$R_{int}(F)$ (%)	17.81
CF (%)	56.426
Structure refinement parameters (<i>SHELXL</i>)	
Data resolution (Å)	1.0
$R_{int}(F^2)$ (%)	15.11
No. of reflections (all)	1269
No. of reflections ($>4\sigma$)	720
$R1$ (4σ) (%)	31.40
$R1$ (all) (%)	38.96
Goodness-of-fit	3.016

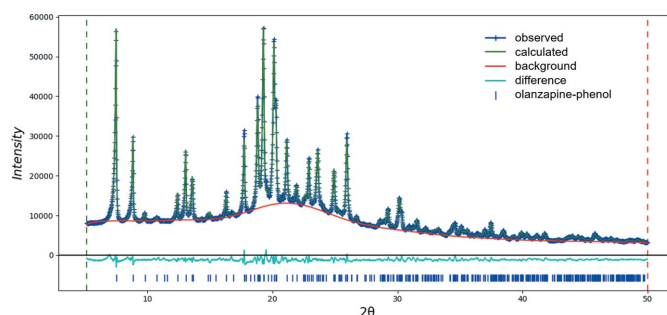


Figure 6
Final fit of the 3D ED structural model against powder XRD data.

imposing constraints on the aromatic ring and all H-atom positions. Additionally, restraints were imposed on other interatomic distances and the planarity of the major flat blocks that make up the molecules. More details of the structure determination and refinement are reported in Table 1. The high values of the agreement parameters can be explained by the relative poor quality of the 3D ED data, which are not suitable for performing an *ab initio* structure solution. Rietveld refinement, starting from the model obtained from the 3D ED data, converged to $R_{wp} = 3.019$, $R_F = 3.849$ and $R_{F2} = 3.512\%$, without any significant modification (Fig. 6). The final structural model is shown in Fig. 7.

The significant difference between the value of unit-cell parameter *a* measured by 3D ED and the value refined by powder XRD can be explained by a vacuum effect on the phenol molecules that are oriented along [100] and partially evaporated upon heating under vacuum.

3.3. Optimization

DFT-D calculations correctly describe the structure with only minor structural differences expected for calculations made with the zero thermal component. A comparison of the experimental and optimized structures shows minor differences in the hydrogen-bond lengths, relative ring angles and phenol position, but leave the overall structure intact, indicating a structural energy minimum (Fig. 8). The output details of the DFT-D calculations are summarized in Table 2.

3.4. Crystal packing and hydrogen bonding

In almost all its known forms (anhydrous and hydrates), olanzapine adopts mirror-related conformations, which rapidly interconvert in solution by inversion of the diazepine ring (Petcher & Weber, 1976). The two enantiomers are packed around crystallographic inversion centres, compelling olanzapine to crystallize in centrosymmetric space groups. Interestingly, no specific intermolecular interactions are needed to stabilize this dimer. According to Reutzel-Edens *et al.* (2003), packing appears to be spatially driven, with complementarity of the opposite enantiomers (electrostatic interaction). Conversely, other researchers (Wawrzycka-Gorczyca

et al., 2004; Ravikumar *et al.*, 2005; Thakuria & Nangia, 2011) associated the pair stability with three types of multiple C—H $\cdots\pi$ contacts (Malone *et al.*, 1997). Independently from the character of the intermolecular interactions, the centrosymmetric dimer observed in most of the olanzapine crystal structures is generally considered to be the building block of

Table 2

Selected parameters from the experimental (3D ED), refined (powder XRD) and optimized (DFT-D) structures.

	3D ED experimental structure	Powder XRD refined structure	DFT-D optimized structure
No. of optimization steps	—	—	98
N \cdots O hydrogen-bond length (Å)	2.891	2.695	2.734
N \cdots N hydrogen-bond length (Å)	3.241	4.224	2.962

the crystal, from which different solid-state structures of olanzapine may be assembled.

Ayala *et al.* (2006) showed that the intermolecular distances in olanzapine structures range from 4.665 to 5.120 Å. The shortest distance corresponds to the pure olanzapine polymorphs, while for hydrates, the extra molecules placed among the centrosymmetric dimers expand their packing. Conversely, in olanzapine–phenol cocrystal described in this article, no expansion was observed and the intermolecular distance is comparable with those of the pure olanzapine polymorphs.

There are four known anhydrous forms of olanzapine. Three of these have been structurally resolved by XRD. The last, labelled as form III, has not been synthesized as a pure phase and has only been reported as a theoretically predicted model (Askin *et al.*, 2019). In anhydrous form I (Wawrzycka-Gorczyca *et al.*, 2004), dimers have a parallel packing (Fig. 9*a*), while in anhydrous form II (Thakuria & Nangia, 2011), dimers have a herringbone arrangement (Fig. 9*b*). Both crystal structures are sustained by an N—H \cdots N hydrogen bond.

The structural model of anhydrous form IV is the only one that does not contain dimer motifs. This structure was first predicted by energy minimization (Bhardwaj *et al.*, 2013) and has only recently been crystallized and refined by Askin *et al.* (2019). Here, single olanzapine molecules are arranged in a

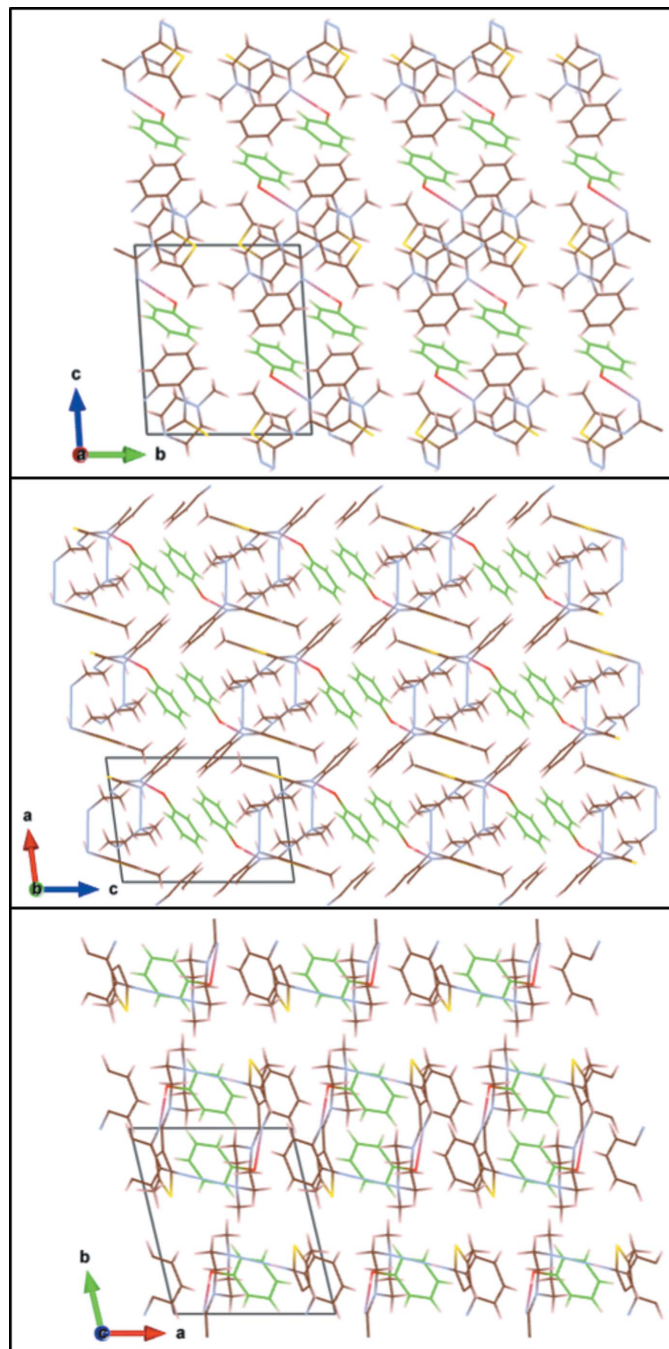


Figure 7

The final structural model of olanzapine–phenol cocrystal, with phenol molecules shown in green. N—H \cdots O hydrogen bonds between olanzapine and phenol molecules are shown in red. Double hydrogen bonding (N—H \cdots N) between two adjacent dimers, involving each olanzapine molecule in two N—H \cdots N hydrogen bonds, is shown in blue.

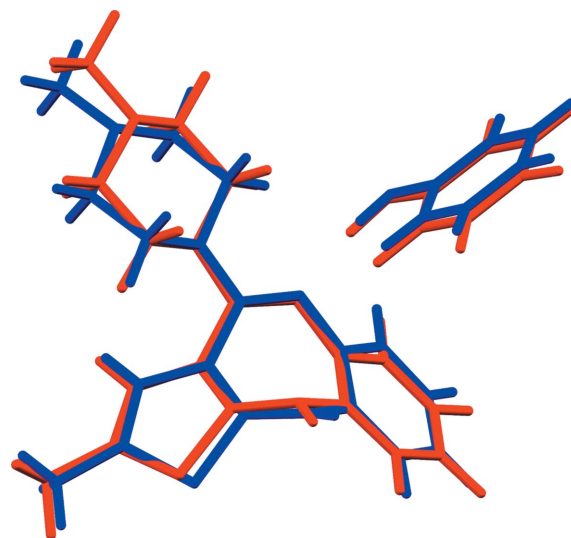


Figure 8

Overlay of the powder XRD refined (blue) and optimized (red) structures of olanzapine–phenol cocrystal.

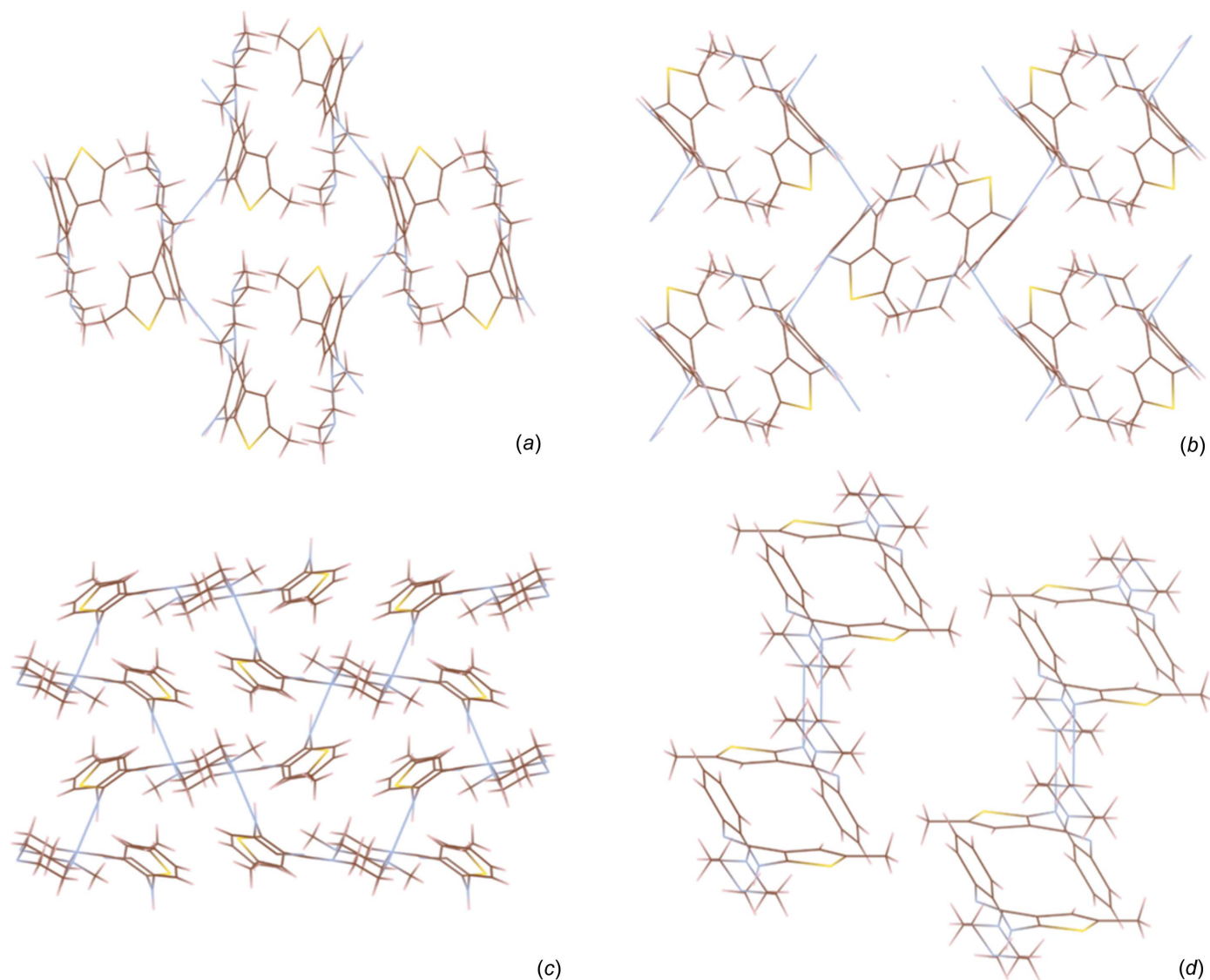


Figure 9
Comparison of the molecular packing in the different crystalline forms of olanzapine: (a) anhydrous form I, (b) anhydrous form II, (c) anhydrous form IV and (d) olanzapine-phenol cocrystal (the phenol molecule is not visualized). N—H...N hydrogen bonds between two adjacent dimers are sketched in blue.

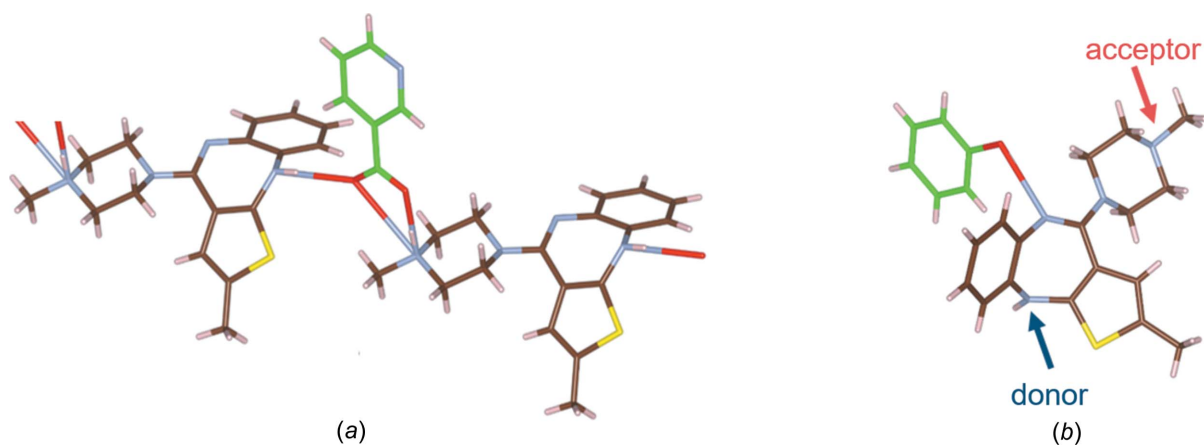


Figure 10
Comparison of the molecular interaction between two 'olanzapine-coformer' structures: (a) intermolecular N—H...O hydrogen bonds in olanzapinium nicotinate and (b) phenol compensation of one olanzapine acceptor in new olanzapine-phenol cocrystal.

ladder-like manner, involving two $N-H \cdots N$ hydrogen bonds, which connect the diazepine $N-H$ donor and the piperazine N -atom acceptor (Fig. 9c).

The hydrogen-bonding arrangements in hydrates are significantly different from those in the pure crystal forms. By incorporating water into the crystal structure, the donor–acceptor ratio becomes balanced, enabling both acceptors on the olanzapine molecule to participate in hydrogen bonding. In all the hydrated systems, the water molecules are held by two or three hydrogen-bonding interactions (Reutzel-Edens *et al.*, 2003).

The only reported ‘olanzapine–coformer’ structure is olanzapinium nicotinate (Ravikumar *et al.*, 2005). The Coulombic interaction between the olanzapinium and nicotinic acid ions is supplemented by intermolecular $N-H \cdots O$ hydrogen bonds, forming catameric chains along the one main axis (Fig. 10a). Olanzapinium dimers here are further stabilized by weak $C-H \cdots \pi$ interactions. There is no direct hydrogen bonding between dimers.

In the case of olanzapine–phenol cocrystal, as in most of the known olanzapine structures, centrosymmetric dimers are present. Additionally, phenol acts as a hydrogen-bond donor for the diazepine N atom, one of the two potential olanzapine acceptors (Fig. 10b). In this way, phenol compensates for the disparity in the ratio of hydrogen-bond donors to acceptors and allows for double hydrogen bonding ($N-H \cdots N$) between two adjacent dimers. Consequently, interdimer connections are guaranteed by double $N-H \cdots N$ hydrogen bonds between two adjacent olanzapine molecules (Fig. 9d). Therefore, the structure consists of continuous dimeric chains stacked along [100]. Additionally, the presence of phenol appears to stabilize the structure in the other directions. Upon heating under vacuum for 7 d, the material assumes the characteristic yellow colour, adopting the structure of anhydrous olanzapine form I.

4. Conclusions

A new olanzapine–phenol cocrystal was discovered as an intermediate product during the crystallization of olanzapine from volatile deep eutectic solvents. The ability of 3D ED to investigate nanocrystalline intermediate forms paves the way for a thorough understanding of the crystallization pathways in pharmaceutical chemistry. Structure solution by single-crystal XRD was not possible due to limited crystals sizes and morphologies, something pervasive throughout organic crystallization. Nevertheless, the structure was solved from electron diffraction data collected from a single nanocrystal using the 3D ED approach. The stability of the result was confirmed by DFT-D structural optimization and the molecular ratio of the cocrystal was confirmed by NMR spectroscopy. The dimeric packing of olanzapine–phenol cocrystal resembles that observed in the three known anhydrous olanzapine polymorphs and differs from that of the hydrated and other cocrystallized forms. Complete information about the intermediate structure of cocrystals during the formation process is essential for discovery of possible new polymorphs, not just of olanzapine, but in any organic system.

Acknowledgements

The authors would like to thank Dr Sean Davis for obtaining the SEM images, and Drs Arianna E. Lanza and Enrico Mugnaioli for assistance and helpful discussions regarding the refinement of the final structure. SRH and JP acknowledge MagnaPharm, a collaborative research project funded by the European Union’s Horizon 2020 Research and Innovation programme (grant No. 736899). IA and MG acknowledge the Regione Toscana for funding the purchase of the Timepix through the FELIX project (POR CREO FERS 2014–2020).

Funding information

The following funding is acknowledged: Horizon 2020 (grant No. 736899); Regione Toscana (grant No. POR CREO FERS 2014–2020).

References

- Andrusenko, I., Hamilton, V., Mugnaioli, E., Lanza, A., Hall, C., Potticary, J., Hall, S. R. & Gemmi, M. (2019). *Angew. Chem.* **131**, 11035–11038.
- Andrusenko, I., Mugnaioli, E., Gorelik, T. E., Koll, D., Panthöfer, M., Tremel, W. & Kolb, U. (2011). *Acta Cryst.* **B67**, 218–225.
- Askin, S., Cockcroft, J. K., Price, L. S., Gonçalves, A. D., Zhao, M., Tocher, D. A., Williams, G. R., Gaisford, S. & Craig, D. Q. M. (2019). *Cryst. Growth Des.* **19**, 2751–2757.
- Ayala, A. P., Siesler, H. W., Boese, R., Hoffmann, G. G., Polla, G. I. & Vega, D. R. (2006). *Int. J. Pharm.* **326**, 69–79.
- Bhana, N., Foster, R. H., Olney, R. & Plosker, G. L. (2001). *Drugs*, **61**, 111–161.
- Bhardwaj, R. M., Price, L. S., Price, S. L., Reutzel-Edens, S. M., Miller, G. J., Oswald, I. D. H., Johnston, B. F. & Florence, A. J. (2013). *Cryst. Growth Des.* **16**, 1047–1055.
- Bitter, I., Dossenbach, M. R. K., Brook, S., Feldman, P. D., Metcalfe, S., Gagiano, C. A., Füredi, J., Bartko, G., Janka, Z., Banki, C. M., Kovacs, G. & Breier, A. (2004). *Prog. Neuropsychopharmacol. Biol. Psychiatry*, **28**, 173–180.
- Bojarska, J., Maniukiewicz, W. & Sieroń, L. (2013). *Acta Cryst.* **C69**, 781–786.
- Burla, M. C., Caliandro, R., Carrozzini, B., Cascarano, G. L., Cuocci, C., Giacovazzo, C., Mallamo, M., Mazzzone, A. & Polidori, G. (2015). *J. Appl. Cryst.* **48**, 306–309.
- Capuano, B., Crosby, I. T., Fallon, G. D., Lloyd, E. J., Yuriev, E. & Egan, S. J. (2003). *Acta Cryst.* **E59**, o1367–o1369.
- Citrome, L., McEvoy, J. P., Todtenkopf, M. S., McDonnell, D. & Weiden, P. J. (2019). *Neuropsychiatr. Dis. Treat.* **15**, 2559–2569.
- Das, P. P., Mugnaioli, E., Nicolopoulos, S., Tossi, C., Gemmi, M., Galanis, A., Borodi, G. & Pop, M. M. (2018). *Org. Process Res. Dev.* **22**, 1365–1372.
- Dovesi, R., Erba, A., Orlando, R., Zicovich-Wilson, C. M., Civalleri, B., Maschio, L., Réat, M., Casassa, S., Baima, J., Salustro, S. & Kirtman, B. (2018). *WIREs Comput. Mol. Sci.* **8**, e1360.
- Duarte, A. R. C., Ferreira, A. S. D., Barreiros, S., Cabrita, E., Reis, R. L. & Paiva, A. (2017). *Eur. J. Pharm. Biopharm.* **114**, 296–304.
- Fedorov, I., Zhuravlev, Y. & Berveno, V. (2012). *Phys. Status Solidi B*, **249**, 1438–1444.
- Fulton, B. & Goa, K. L. (1997). *Drugs*, **53**, 281–298.
- Gemmi, M. & Lanza, A. E. (2019). *Acta Cryst.* **B75**, 495–504.
- Gemmi, M., Mugnaioli, E., Gorelik, T. E., Kolb, U., Palatinus, L., Boullay, F., Hovmöller, S. & Abrahams, J. P. (2019). *ACS Cent. Sci.* **5**, 1315–1329.

- Georgieva, D., Jansen, J., Sikharulidze, I., Jiang, L., Zandbergen, H. W. & Abrahams, J. P. (2011). *J. Instrum.* **6**, C01033.
- Grimme, S. (2006). *J. Comput. Chem.* **27**, 1787–1799.
- Groom, C. R., Bruno, I. J., Lightfoot, M. P. & Ward, S. C. (2016). *Acta Cryst.* **B72**, 171–179.
- Infantes, L., Fábrián, L. & Motherwell, W. D. S. (2007). *CrystEngComm*, **9**, 65–71.
- Kirkpatrick, S., Gelatt, C. D. Jr & Vecchi, M. P. (1983). *Science*, **220**, 671–680.
- Lanza, A., Margheritis, E., Mugnaioli, E., Cappello, V., Garau, G. & Gemmi, M. (2019). *IUCrJ*, **6**, 178–188.
- Malone, J. F., Murray, C. M., Charlton, M. H., Docherty, R. & Lavery, A. J. (1997). *J. Chem. Soc. Faraday Trans.* **93**, 3429–3436.
- Nanubolu, J. B. & Ravikumar, K. (2017). *CrystEngComm*, **19**, 355–366.
- Palatinus, L., Brázda, P., Jelínek, M., Hrdá, J., Steciuk, G. & Klementová, M. (2019). *Acta Cryst.* **B75**, 512–522.
- Petcher, T. J. & Weber, H.-P. (1976). *J. Chem. Soc., Perkin Trans. II*, pp. 1415–1420.
- Potticary, J., Hall, C., Hamilton, V., McCabe, J. F. & Hall, S. R. (2020). *Cryst. Growth Des.* **20**, 2877–2884.
- Ravikumar, K., Swamy, G. Y. S. K., Sridhar, B. & Roopa, S. (2005). *Acta Cryst.* **E61**, o2720–o2723.
- Reutzel-Edens, S. M., Bush, J. K., Magee, P. A., Stephenson, G. A. & Byrn, S. R. (2003). *Cryst. Growth Des.* **3**, 898–907.
- Rojo, L. E., Gaspar, P. A., Silva, H., Risco, L., Arena, P., Cubillos-Robles, K. & Jara, B. (2015). *Pharmacol. Res.* **101**, 74–85.
- Sarmah, K. K., Sarma, A., Roy, K., Rao, D. R. & Thakuria, R. (2016). *Cryst. Growth Des.* **16**, 1047–1055.
- Sheldrick, G. M. (2015). *Acta Cryst.* **C71**, 3–8.
- Thakuria, R. & Nangia, A. (2011). *Acta Cryst.* **C67**, o461–o463.
- Toby, B. H. & Von Dreele, R. B. (2013). *J. Appl. Cryst.* **46**, 544–549.
- Wawrzycka-Gorczyca, I., Koziol, A. E., Glice, M. & Cybulski, J. (2004). *Acta Cryst.* **E60**, o66–o68.
- Zhang, Y.-B., Su, J., Furukawa, H., Yun, Y., Gándara, F., Duong, A., Zou, X. & Yaghi, O. M. (2013). *J. Am. Chem. Soc.* **135**, 16336–16339.